Comparison of astrospheres around cool and hot stars

2016 J. Phys.: Conf. Ser. 767 012024

(http://iopscience.iop.org/1742-6596/767/1/012024)

Journal of Physics: Conference Series **767** (2016) 012024 doi:10.1088/1742-6596/767/1/012024

Comparison of astrospheres around cool and hot stars

K. Scherer[1,2], D.J. Bomans[3,2], S.E.S. Ferreira[4], H. Fichtner[1,2], J. Kleimann[1], R.D. Strauss[4], K. Weis[3]

[1] Institut für Theoretische Physik IV: Weltraum- und Astrophysik, Ruhr-Universität Bochum, Germany
[2]Research Department, Plasmas with Complex Interactions, Ruhr-Universität Bochum, Germany
[3]Astronomische Institute, Ruhr-Universität Bochum, Germany
[4]Center for Space Research, North-West University, 2520 Potchefstroom, South Africa

E-mail: kls@tp4.rub.de

Abstract. Simulations of astrospheres around hot and cool stars have recently move into the focus of scientific research. We describe here the differences between the astrospheres around hot and cool stars. While those around the former are huge (on pc scales) because of their high stellar wind momentum flow, those around cool stars are on a AU scale and the heliosphere can be used as a standard. Here, we will compare the differences and commonalities between such astrospheres.

1. Introduction

Every supersonic wind-driving star moving supersonically (superalvfénically) through the interstellar medium exhibits a bow shock, an astropause and a terminations shock. The mass flux of stellar winds around cool stars (mainly F,G,K stars) is usually small compared of those around hot stars (O and B stars). The most detailed observations of an astrosphere around a cool star are available for the heliosphere, the astrosphere around the Sun. Especially due to the Voyager 1 spacecraft we have nowadays in situ observations from the region beyond the heliopause (astropause). Some astrospheres of nearby cool stars could be observed in the Lyman-α line [1, 2], the observations of the astrospheres of hot stars are mainly based on Hα light (e.g., [3]). To understand these other astrospheres one has to transfer our detailed knowledge of the heliosphere. But this has to be done with some care, because radiative cooling plays an important role in the physics of astrospheres around hot stars, for which the characteristic length scales are parsec, compared to hundreds of AU for those around cool stars.

In the following we use a model of the heliosphere as example for an astrosphere around a cool star, which we compare to that of the astrosphere around the hot O star λ Cephei.

2. Astrosphere models

To model astrospheres we use the set of ideal Euler equations described in [4], in case of hot stars including cooling and heating functions in the energy equation. While the ideal hydrodynamic (HD) and and magneto-hydrodynamic (MHD) Euler equations are scale-invariant, this property

is lost when adding either cooling and heating functions or a neutral component. Nevertheless, it is in principle possible to use scale-invariance to compare astrospheres around cool and hot stars, keeping in mind that this is only approximately true.

Thus neglecting the influence of neutrals and using the fact that cooling and heating functions are not effective for cool star astrospheres, they can be modeled using ideal MHD, and the heliosphere is used as the standard. For the astrospheres around hot stars we use the O star λ Cephei with cooling and heating, also neglecting neutrals because of the high flux of ionizing photons.

2.1. The heliosphere

The heliospheric large-scale structures is described with HD or MHD models of increasing complexity (e.g., [5, 6, 7, 8, 9, 10, 11, 12]). We base our simulations on the Cronos code with ideal (M)HD [13, 14, 15, 11, 4] using the following parameters [8] at 1 AU: $v_{\rm sw} = 375$ km/s, $n_{\rm sw} = 7$ cm^{-3}, $T_{\rm sw} = 7.364 \times 10^4$ K, whereas those for the ISM are $v_{\rm ism} = 26.4$ km/s, $n_{\rm ism} = 0.06$ cm^{-3}, and $T_{\rm ism} = 6.53 \times 10^3$ K. As usual, an axisymmetric configuration forms, which is characterized by the termination shock (TS) terminating the supersonic solar/stellar wind, a bow shock (BS) on the upwind side, where the interstellar flow (as seen in the rest frame of the Sun/star) changes from supersonic to subsonic speed, and a tangential discontinuity, the helio-/astropause (HAP) in between. The inner helio-/astrosheath (IHAS) is the region between the TS and the HAP, and the outer helio-/astrosheath (OHAS) that between the HAP and the BS (see Fig. 1). The bow shock may not exist, when the fast magnetosonic wave speeds are higher than the inflow speed [16, 17], but see also [18], who pointed out that heavier elements can lower the fast magnetosonic speed.

To be comparable with the O-star astrosphere, we refer here to a heliosphere without neutral interaction, that is the local ISM is completly ionized. It is very propable that the heliosphere has or will pass through Such an environement during its passage around the galactic center [19]. Because the heliosphere is small compared to O-star astrospheres heating or coolling (described below) does not play a role.

2.2. λ Cephei

In [20] we discussed in detail the hydrodynamic structure of the astrosphere of λ Cephei. In Fig. 1 we now present a MHD model of λ Cephei: the stellar magnetic field is assumed to be 100 times large than the solar field [21], and a hypothetical spiral field at 1 AU is then also 100 times stronger. This hypothetical field is then transported as a spiral magnetic field after [22] to the inner boundary at 0.03 pc. For the undisturbed interstellar magnetic field (IMF) we assumed a strength of 10 μG [23], and a field orientation deviating from the inflow direction (along the x-axis) by 45° in both φ and ϑ. Because the ram pressure of the interstellar medium (ISM) $\rho_{ism} v_{ism}^2$ (with the ISM density $\rho/m_p = 11\,\mathrm{cm}^{-3}$, $v_{ism} = 80\,\mathrm{km/s}$ and m_p is the proton mass) is higher than that of the IMF:

$$\beta = \frac{8\pi\rho_{ism} v_{ism}^2}{B_{ism}^2} \approx 280 \tag{1}$$

there is only negligible dynamical influence of the magnetic field and the λ Cephei astrosphere is quite similar to a single-fluid hydrodynamic one. During the modeling it turned out that the cooling function by [24] leads to unstable results, thus we used for the recent calculation that by [25]. The model is shown in Fig. 1.

2.3. Comparison of the cool and hot models

2.4. The HD structure

For ideal HD shocks the structure of the heliosphere is well known (see [4] for an overview). On

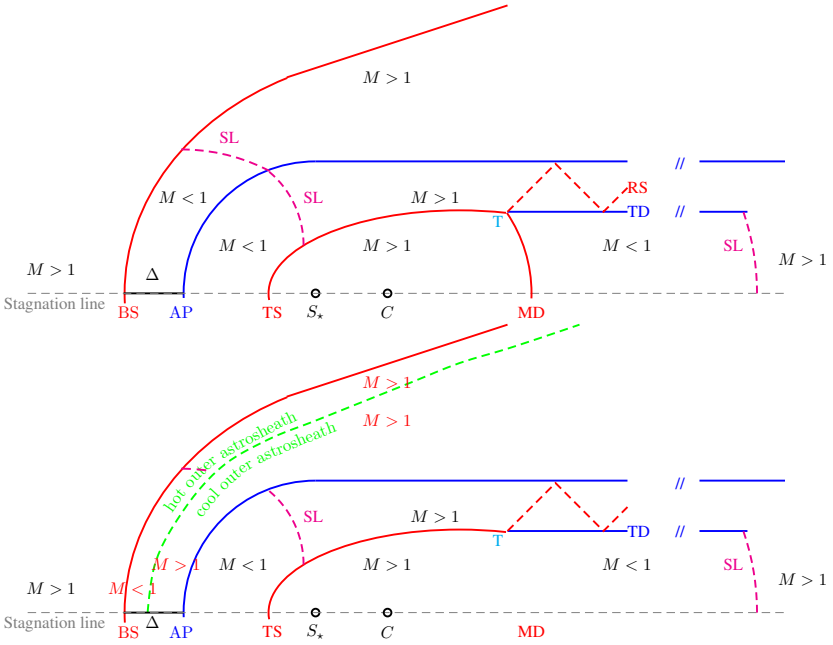

Figure 1. The standard HD model without cooling is shown in the upper panel. The star $S_\star$ is at the origin, SL denotes the sonic line, BS, AP, and TS are the bow shock, astropause and termination shock, MD is the spherical Mach disk, with origin at C, TD and RS are the triple point and an additional tangential discontinuity. M is the Mach number and Δ the distance between BS and AP (see [4] for details). Astrospheres including cooling (lower panel) show an additional feature: the outer astrosheath is split in a cool and a hot one.

the contrary, astrospheres around hot stars with cooling functions show an additional feature, a cool outer region between the bow shock and the astropause (the cool outer astrosheath, COA) together with a hot region directly after the bow shock (the hot outer astrosheath, HOA) [26, 4]. The reason is that the cooling length is much shorter than the distance Δ between the bow shock and the astropause. This cooling results also in an huge increase in the number density close to the astropause in the outer astrosheath. The cooling is also responsible for a shrinking of the bow shock-astropause distance, see e.g., [4]

2.5. The MHD structure

In Fig. 2 we show a the model of the cool astrosphere in the left panel and that of the hot astrosphere in the right panel. It can be clearly seen that the heliosphere is much more asymmetric than the λ Cephei astrosphere. The reason is that in the ISM of the latter the ram pressure dominates the magnetic field pressure. The ratio of these pressure, the plasma β is usually used to describe the plasma properties. The ratio of the thermal pressure to that of the magnetic field is valid in subsonic flows, but extending the fraction with the ram pressure, we can use it also in the supersonic case:

$$\beta = \frac{8\pi P}{B^2} = \frac{2}{\gamma}\frac{\gamma P}{v^2\rho}\frac{4\pi\rho v^2}{B^2} = \frac{2}{\gamma}\frac{M_A^2}{M_c^2} = \frac{2}{\gamma}\frac{v_c^2}{v_A^2} \tag{2}$$

with the Alfvén speed v_A, the sound speed v_c, and the respective Mach numbers M_A, M_c. The values are displayed in Table 1. It can be seen that for the ISM around the heliosphere the plasma β is small, while for that around λ Cephei is larger than one. Thus the ram pressure is dominated by the magnetic field pressure in the case of the heliosphere while it dominates that of the magnetic field in the case of λ Cephei. Therefore, the heliosphere is asymmetric because of the asymmetric magnetic field pressure, while the λ Cephei astrosphere is symmetric because here the symmetric ram pressure dominates.

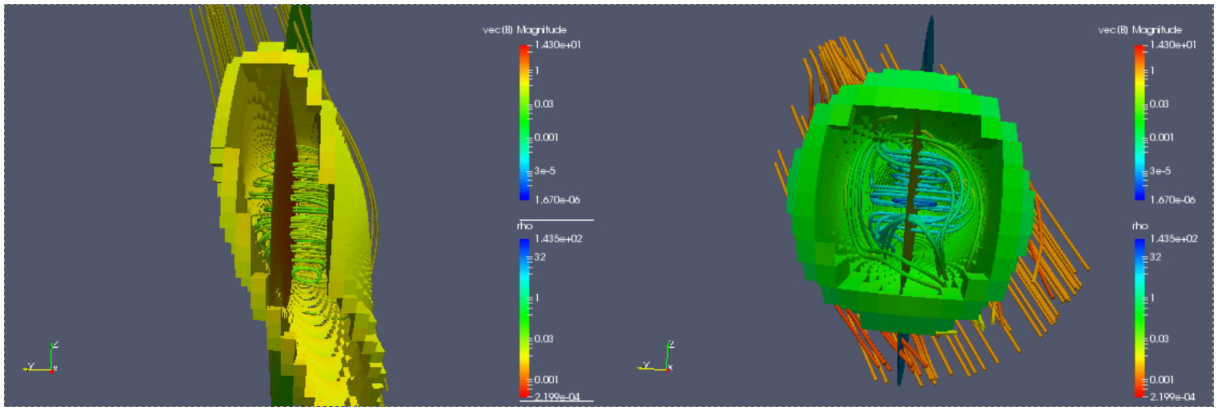

Figure 2. MHD model of the heliosphere (left panel) and λ Cephei (right panel). The star is in the origin. The solid (yellow and green) walls are the region where the number density is between 0.01 and 0.5 cm^{-3}, which is approximately the astropause in both cases. The tubes are the magnetic field lines, and the plane is perpendicular to the inflow. The axis orientation is given in the lower left corner in both panels. In the left figure one sees nicely the inner part with Parker type field lines (the closed ones) and the wrapping of field lines around the heliopause.

Table 1. Comparision of the charateristic parameters between the helio- and an astrosphere.

	heliosphere	astrosphere	
V_A	27.3	6.7	km/s
c_s	9.5	11.4	km/s
M_A	0.97	11.9	
M_c	2.8	7.0	
β	0.14	3.5	

Also in the MHD model the distance between the bow shock and the astropause decreases when cooling is effective (not shown here).

3. Recombination rate

We are here only interested in the projection of a model astrosphere onto the sky, thus we do not discuss the details of the λ Cephei model. But take the number density n and temperature T of the model to calculate the Hα volume recombination rate R:

$$R = 2 \cdot 10^{-10} T^{-4/3} n^2 dr [cm^3 s^{-1}] \tag{3}$$

while dr is the path element chosen to be constant. In principle, one has to calculate the path dr throughout each cell, but the error assuming a constant dr is sufficiently small for the approach described below, because we are only interested in the principle effects.

Because of the low β the compression ratio of the ISM is about 20 similar to the hydrodynamic model, see [20]. The number densities between the bow shock and the astropause range from 44 to 240 cm^{-3}. In this region, the COA, the temperature is similar to that in the ISM, and thus from this region, the highest flux of Hα radiation is emitted. This is easily explained by Eq. 3 which is proportional to the square of the density and decays with the temperature to power -4/3. Thus in the region between the astropause and the termination shock, the region of the shocked stellar wind, the recombination rate can be neglected, because of number densities

below $10^{-2}\,\mathrm{cm}^{-3}$ and temperatures above $10^7\,\mathrm{K}$. Because of the high photon flux close to the star we can neglect the recombination rate inside the termination shock as well. The recombination rate in the ISM is at least a factor 16 lower than in the COA. From our line-of-sight (LOS) integrations we found, that the contribution of he other regions is orders of magnitudes below that of the COA. Thus, we can safely neglect them, and in the following we present only the recombination rate in the COA.

4. Rotations

We shifted the model data to its position in the sky (distance 600 pc, $b = 2.61°$, $l = 103.83°$) and rotated it around the y- and z-axis in steps of 45° each. Because the model is approximately symmetric around the x-axis a rotation about this axis does not give new information and thus is left out here. Nevertheless, if the axisymmetry around the x-axis is broken, these rotations needed to be discussed also (see for example heliospheric models by [27], [28]) Due to the small

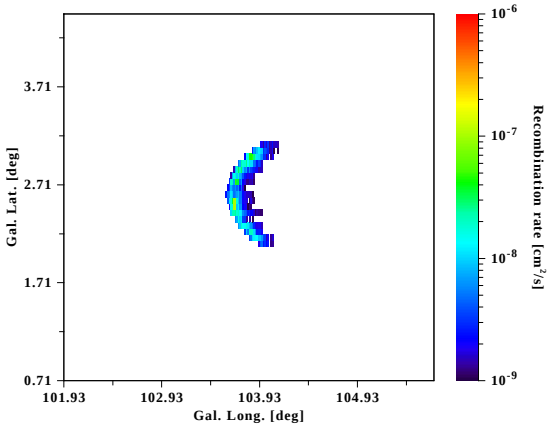

Figure 3. The projection of the λ Cephei MHD model onto the sky. The x- and y-axes denote the galactic longitude and latitude. The color bar gives the logarithmic column recombination rate in cm^2/s. This shape is not rotated.

projection area of $\approx 3° \times 3°$ on the sky, perspective distortions can be neglected, allowing for the use of a simple orthographic projection. In Fig. 3 we show the projection of λ Cephei with no rotation.

In Fig. 4 we show the rotated astrosphere, but without any notation on the axes, because we are only interested in the shape. The axes notation are the same as in Fig 2. The rotation is denoted by the triple (α, δ, γ), where α, δ, and γ are the rotation angles around the x-,y-, and z-axis, respectively.

In Fig. 4 we show the rotation around the z-axis in steps of 45°

A more detailed discussion for these projection features will be given in an upcoming publication.

With these simple rotations, we can get structures, like [29] described for the Herschel infrared observations as "fermata" and "irregular". The "eyes" and "rings" we do not see, because for the eyes we have to include an inner region, and especially the star itself, and the rings are astrospheres with no relative motion with respect to the ISM.

Some of the projections presented above do even look like a bow shock structure.

5. Cosmic rays

In [30] we discuss the propagation of high energetic cosmic rays (above TeV) through an λ Cephei like astrosphere 600 pc away from the observer. We found that such an obstacle modulates the cosmic ray flux (CRF) at the observer. In Fig. 5 a variation along the azimuthal angle is shown where the astrosphere is located at 45^o and the above mentioned distance. It can be seen

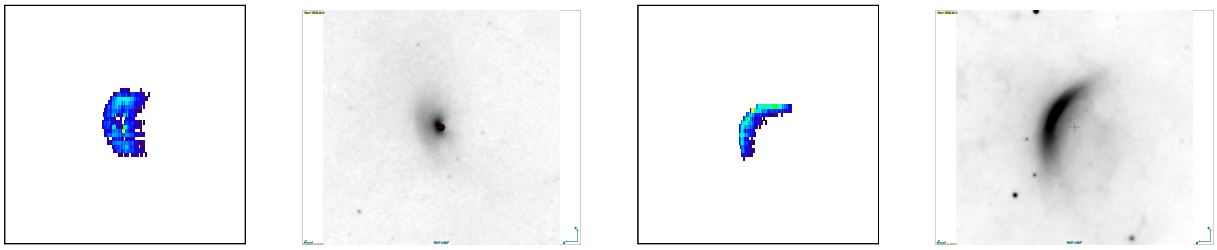

Figure 4. Rotation around the z-axis and observed bow shocks. The rotation angles are given in the brackets **below the panels as well as the identifier for the stars. Both images are obtained in the WISE 22μ infrared band and closely resemble the basic structure of one projected line emission image. The large scale morphology of the WISE 22μ images correlate reasonable well with the morphology observed in ionized gas (Bomans et al., in prep.) and can therefore be used as proxy for ionized gas.**

that there is a variation in the 0.1% range as observed by the large area telescopes e.g., [31]. Moreover, the minimum of the CRF is not at the position of the obstacle. The reason is that

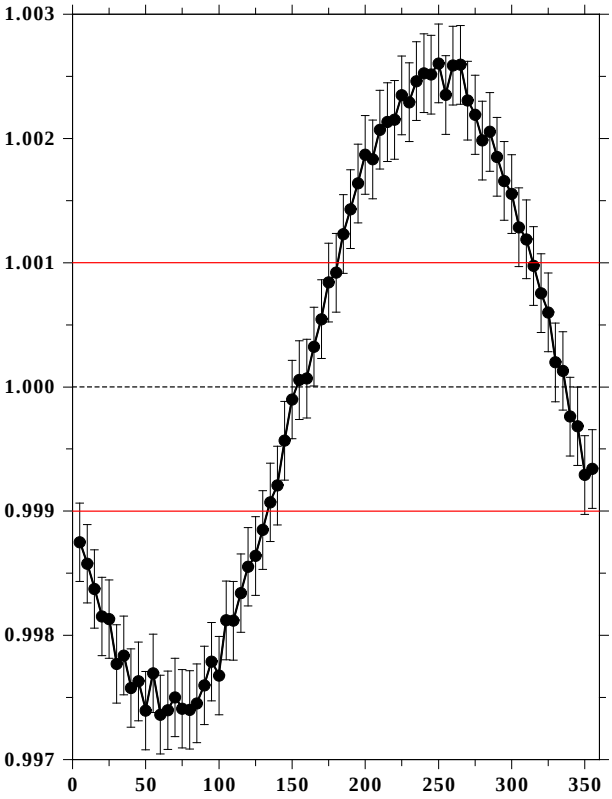

Figure 5. Variation of the cosmic ray flux at Earth for an obstacle with a radius of 10 pc at 600 pc and an angular offset of 45^o. On the x-axis the observer angle ϕ is given, while on the y-axis the relative flux variation is shonw. To guide the eye the two red lines denote the 0.1% level.

the perpendicular diffusion cannot be detected due to the magnetic field being aligned along the y-axis. Due to the latter the position of the minimum CRF varies with the position of the obstacle, for details see [30].

6. Conclusion

We have used a model of λ Cephei to study the projection effects of astrospheres onto the sky. We find that with a single model the principle shapes of a lot of astrospheres can be explained

including asymmetric and irregular ones. We have integrated the Hα recombination rate, which gives a nice representation of the cool outer astrosheath in the Hα light. It may be possible to use other processes, like bremsstrahlung in the hot inner astrosheath, a region, where the stellar wind is subsonic but the temperatures are above 10^7 K.

The astrospheres around hot stars can also act as sinks for the high energy cosmic ray flux.

Acknowledgments

This work was carried out within the framework of the bilateral BMBF-NRF-project 'Astrohel' (01DG15009) funded by the Bundesministerium für Bildung und Forschung. The responsibility of the contents of this work is with the authors. KS, HF, and JK are grateful to the *Deutsche Forschungsgemeinschaft (DFG)* funding the projects SCHE334/9-1, SCHE334/9-2, and FI706/15-1.

References

[1] Wood B E, Izmodenov V V, Linsky J L and Alexashov D 2007 *Astrophys. J.* **659** 1784–1791 (*Preprint* `arXiv:astro-ph/0701274`)
[2] Linsky J L and Wood B E 2014 *ASTRA Proceedings* **1** 43–49 (*Preprint* `1408.5934`)
[3] Brown D and Bomans D J 2005 *Astron. Astrophys.* **439** 183–194
[4] Scherer K, Fichtner H, Kleimann J, Wiengarten T, Bomans D J and Weis K 2016 *Astron. Astrophys.* **586** A111 URL `http://dx.doi.org/10.1051/0004-6361/201526137`
[5] Pauls H L and Zank G P 1996 *J. Geophys. Res.* **101** 17081–17092
[6] Fahr H J, Kausch T and Scherer H 2000 *Astron. Astrophys.* **357** 268–282
[7] Borrmann T and Fichtner H 2005 *Adv. Space Res.* **35** 2091–2101
[8] Müller H R, Florinski V, Heerikhuisen J, Izmodenov V V, Scherer K, Alexashov D and Fahr H J 2008 *Astron. Astrophys.* **491** 43–51 (*Preprint* `0804.0125`)
[9] Arthur S 2007 *Rev. Mex. Astron. Astrophys.* **30** 64–71
[10] Izmodenov V V, Alexashov D B and Ruderman M S 2014 *Astrophys. J. Lett.* **795** L7 (*Preprint* `1409.8128`)
[11] Scherer K, van der Schyff A, Bomans D J, Ferreira S E S, Fichtner H, Kleimann J, Strauss R D, Weis K, Wiengarten T and Wodzinski T 2015 *Astron. Astrophys.* **576** A97 (*Preprint* `1502.04277`)
[12] Zank G P 2015 *Ann. Rev. Astron. Astrophys.* **53** 449–500
[13] Kissmann R, Kleimann J, Fichtner H and Grauer R 2008 *Mon. Not. R. Astron. Soc.* **391** 1577–1588 (*Preprint* `0901.4495`)
[14] Kleimann J, Kopp A, Fichtner H and Grauer R 2009 *Annales Geophysicae* **27** 989–1004
[15] Wiengarten T, Fichtner H, Kleimann J and Kissmann R 2015 *Astrophys. J.* **805** 155 (*Preprint* `1504.01858`)
[16] McComas D J, Alexashov D, Bzowski M, Fahr H, Heerikhuisen J, Izmodenov V, Lee M A, Möbius E, Pogorelov N, Schwadron N A and Zank G P 2012 *Science* **336** 1291–
[17] Zank G P, Heerikhuisen J, Wood B E, Pogorelov N V, Zirnstein E and McComas D J 2013 *Astrophys. J.* **763** 20
[18] Scherer K and Fichtner H 2014 *Astrophys. J.* **782** 25 (*Preprint* `1312.1197`)
[19] Frisch P C 2006 *Solar Journey: The Significance of our Galactic Environment for the Heliosphere and Earth* (Edited by Priscilla C. Frisch, Astrophysics and Space Science Library, Vol. 338. Springer Dordrecht)
[20] Scherer K, Fichtner H, Fahr H J and Röken C 2015 *Submitted to Astrophys. J.*
[21] Walder R, Folini D and Meynet G 2012 *Space Sci. Rev.* **166** 145–185 (*Preprint* `1103.3777`)
[22] Parker E N 1963 *Interplanetary dynamical processes.* (New York, Interscience Publishers, 1963.)
[23] Beck R 2012 *Space Sci. Rev.* **166** 215–230
[24] Siewert M, Pohl M and Schlickeiser R 2004 *Astron. Astrophys.* **425** 405–416 (*Preprint* `astro-ph/0409075`)
[25] Schure K M, Kosenko D, Kaastra J S, Keppens R and Vink J 2009 *Astron. Astrophys.* **508** 751–757 (*Preprint* `0909.5204`)
[26] Mackey J, Gvaramadze V V, Mohamed S and Langer N 2015 *Astron. Astrophys.* **573** A10 (*Preprint* `1410.0019`)
[27] Pogorelov N V, Borovikov S N, Zank G P and Ogino T 2009 *Astrophys. J.* **696** 1478–1490
[28] Opher M 2012 *The Astronomical Review* **7** 010000–78
[29] Cox N L J, Kerschbaum F, van Marle A J, Decin L, Ladjal D, Mayer A, Groenewegen M A T, van Eck S, Royer P, Ottensamer R, Ueta T, Jorissen A, Mecina M, Meliani Z, Luntzer A, Blommaert J A D L, Posch T, Vandenbussche B and Waelkens C 2012 *Astron. Astrophys.* **543** C1

[30] Scherer K, Fichtner H, Kleimann J, Wiengarten T, Bomans D J and Weis K 2016 *Astron. Astrophys.* **586** A111 (*Preprint* 1512.01089)
[31] IceCube Collaboration, Aartsen M G, Abraham K, Ackermann M, Adams J, Aguilar J A, Ahlers M, Ahrens M, Altmann D, Anderson T and et al 2016 *ArXiv e-prints* (*Preprint* 1603.01227)